HAL
open science

Experimental and modeling study of the oxidation of fenchone, a high-energy density fuel-additive

L. Boualem, Z. Serinyel, A. Nicolle, M. Lailliau, P. Dagaut, G. Dayma

To cite this version:

L. Boualem, Z. Serinyel, A. Nicolle, M. Lailliau, P. Dagaut, et al.. Experimental and modeling study of the oxidation of fenchone, a high-energy density fuel-additive. Fuel, 2023, 353, pp.129183. 10.1016/j.fuel.2023.129183 . hal-04164151

HAL Id: hal-04164151

https://hal.science/hal-04164151v1

Submitted on 19 Jul 2023

HAL is a multi-disciplinary open access archive for the deposit and dissemination of scientific research documents, whether they are published or not. The documents may come from teaching and research institutions in France or abroad, or from public or private research centers.

L'archive ouverte pluridisciplinaire **HAL**, est destinée au dépôt et à la diffusion de documents scientifiques de niveau recherche, publiés ou non, émanant des établissements d'enseignement et de recherche français ou étrangers, des laboratoires publics ou privés.

Copyright

EXPERIMENTAL AND MODELING STUDY OF THE OXIDATION OF FENCHONE, A HIGH-ENERGY DENSITY FUEL-ADDITIVE

L. Boualem*, **, Z. Serinyel*, **, A. Nicolle*, M. Lailliau*, **, P. Dagaut** and G. Dayma*, ****

guillaume.dayma@cnrs-orleans.fr

*Université d'Orléans, Château de la Source, avenue du Parc Floral, 45067 Orléans, France

**ICARE–CNRS, 1c avenue de la recherche scientifique, 45071 Orléans, France

***Aramco Fuel Research Center, 232 avenue Napoleon Bonaparte, 92852 Rueil-Malmaison, France

Abstract

Increasing fuel energy density constitutes a potential way to reduce engine exhaust carbon emission. Fenchone, a strained ring molecule, could be an interesting candidate. The present study investigates the oxidation of fenchone in a jet-stirred reactor at high pressure (10 atm) between 700 and 1180 K at constant fuel mole fraction and constant residence time of 0.1% and 0.7 s, respectively. Mole fraction profiles were obtained through sonic probe sampling, and analyzed by gas chromatography and Fourier transform infrared spectrometry. More than 30 species were identified and most of them were quantified. Also, a kinetic mechanism is developed in this study and tested against the present conditions showing good agreement. The present mechanism allows to illuminate the major reaction pathways involved in the decomposition routes of the fuel and its primary radicals as well as the formation pathways of the quantified intermediate species. During fenchone oxidation, the carbonyl group is mostly found in CO, CO_2 and formaldehyde while heavier carbonyl species were identified at much lower quantities, indicating decarbonylation occurs early during the oxidation process.

Aromatic compounds such as benzene and toluene are formed especially in rich conditions while some potential oxygenated pollutants like methacrolein and acetaldehyde were quantified as well.

1. Introduction

Reformulation of transportation fuels through the incorporation of low-carbon blendstocks such as electrofuels constitutes an important option to address the pressing climate challenges [1]. The potential use of blendstocks and additives requires an in-depth knowledge of the combustion kinetics of the emerging components as well as of the nature and quantity of pollutants formed during their oxidation and thermal decomposition.

Strained ring hydrocarbons (SRH) are of interest as high-energy density components in transportation systems. These are readily produced from renewable feedstocks [2]. However, the impact of SRH on soot characteristics remains unclear [3], the respective importance of cyclopentadiene, fulvene and other benzene production routes being strongly dependent on combustion conditions [4]. Abdrabou et al. [5] showed that norbornane addition to a Diesel fuel involves a threshold soot index reduction and soot disorder increase, as a result of five-membered ring incorporation in the molecular structure of soot [6, 7]. Functionalizing SRH with oxygen-containing groups, such as alcohols or ketones, may help in further reducing SRH sooting propensity [8], however at the expense of the SRH calorific value. In a recent study by Morajkar et al. [9], the effect of the addition of solid camphor and camphor oil to Diesel fuel on its sooting propensity is studied using a diffusion flame. The authors reported physicochemical changes such as a smaller particle diameter in the presence of camphor, which they linked to the increased oxidative reactivity.

Combustion characteristics of the SRH is insufficiently addressed. Among these hydrocarbons, JP-10 (mostly endo-tetrahydrodicyclopentadiene), produced by the catalytic hydrogenation of dicyclopentadiene, is probably the most studied one; e.g. [4, 10-12]. The aim of the present work is to study experimentally the combustion mechanism of fenchone (1,3,3-trimethyl-bicycloheptan-2-one), a monoterpenoid present in fennel oil, and to provide a predictive pollutant formation model in oxygenated SRH combustion, opening up the use of such SRH for specific transport applications. Table 1 presents a comparison between octane number (RON, MON), lower heating value (LHV), and boiling point for fenchone and few other popular additives.

Fenchone can be found in wormwood with a concentration lower than 5 mg L^{-1}. It can also be found in essential oils extracted from fennel seeds in varying concentrations depending on the species of fennel and its growing place. According to the European Pharmacopoeia, the essential oil of bitter fennel produced from the aerial parts of the plant (Foeniculum Vulgare) may contain between 7 and 25% of fenchone. This monoterpene is used as a raw material for the manufacture of flavours in food and perfumery. It can also be used in beverages as a preservative or in detergents and soaps.

The only combustion-related study on fenchone goes back to 2014, which reports the laminar flame speeds of fenchone at 453 K [13]. Their results suggest that the laminar flame speeds of fenchone are close to those of JP-10 previously measured by Parsinejad et al. [12], on the lean side and very close to those of α-pinene [14]. To the best of our knowledge, except flash pyrolysis experiments performed in the 1960's [15], there are no oxidation or pyrolysis studies reporting intermediate species, hence providing details on fenchone decomposition routes.

Table 1: Main characteristics of some popular additives.

Compound	RON [16]	MON [16]	LHV (MJ/kg) [17]	BP (°C)
fenchone	93	81	38	192
diisopropylketone	102	93	36	125
2-butanone	109	104	32	80
isobutanol	103	91	33	108
cyclopentanone	103	90	32	131

The molecular structure of fenchone is illustrated in Figure 1. Among the high-density hydrocarbon fuels, structural similarities can be drawn between fenchone and norbornane (as well as 2-ethylnorbornane) for which limited theoretical studies exist. For example, recently Wang et al. [18] calculated the bond energies of 2-ethylnorbornane, norbornadiene and quadricyclane at the CCSD(T)/cc-PVTZ//B3LYP/6-311++g(d,p) level of theory. According to their calculations and based on similarities, F2 (see Fig. 1 for radicals' names) is the least likely radical to be formed with a C–H bond energy around 107 kcal mol^{-1} followed by F1 with 104–105 kcal mol^{-1}. On the other hand, C–H bonds at positions F5–F6 (101.4 kcal mol^{-1}) and F3–F4 (98.7 kcal mol^{-1}) are quite similar to primary (~101 kcal mol^{-1}) and secondary (~98.5 kcal mol^{-1}) C–H bond energies in alkanes.

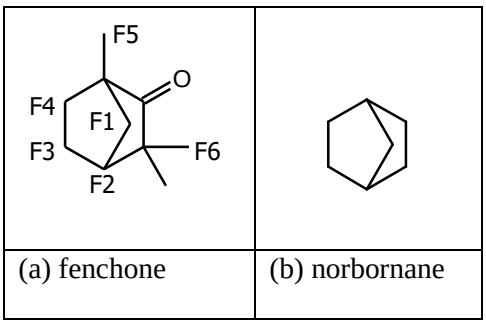

(a) fenchone (b) norbornane

Figure 1. Structure of fenchone (a), and norbornane (b). Fx denotes the name of the radical in the mechanism according to the position of the free electron.

Sirjean et al. [19] used ab initio methods to calculate some important reaction rate constants in the decomposition of norbornane, at the CBS-QB3 level of theory. In Sirjean et al. [19], the spin-contamination energy correction which they proposed pertains to biradicals which are not considered in the present study. No symmetry correction to CBS-QB3 values were necessary either as the structures considered are not symmetric, unlike some species featured in Sirjean's study. The lowest energy conformer obtained by MMFF94 optimization was used as a guess for CBS-QB3 calculations within the RRHO approximation. As radical formation enthalpies are deduced from reference (fenchone) value and difference of CBS-QB3 enthalpies, the remaining errors (estimated to be lower than 2 kcal mol^{-1}) should partially cancel out between the structures calculated. Regarding isodesmic reactions, fenchone standard formation enthalpy was calculated using the following reaction: fenchone + 3 propane ⇌ norbornane + acetone + neopentane + isobutane. Given that there are no theoretical studies in the literature on fenchone oxidation and ab initio rate constant calculation was outside of the scope of the present study, structure/reactivity analogies were made for the mechanism development (see section 3).

In the present study, oxidation experiments of dilute fenchone/O_2/N_2 mixtures were carried out in a jet-stirred reactor at equivalence ratios of 0.5–2 and at 10 atm, between 700–1180 K, with 1000 ppm as an initial mole fraction of fenchone. Reactants, products and intermediate species were measured and quantified. A kinetic mechanism is developed in order to understand the oxidation pathways of fenchone.

2. Experimental set-up

The present experiments were performed in a jet-stirred reactor, described in detail elsewhere. The reactor used for this study has been described by Dagaut et al. [20]. It is a 4 cm diameter fused-silica sphere (42 cm^3) with four injectors (nozzles of 1 mm I.D). This apparatus has been

designed to provide stirring under the present conditions. An HPLC pump (LC10 AD VP) with an online degasser (Shimadzu DGU-20 A3) was used to inject 1000 ppm of fenchone (>99% pure from Aldrich, L-fenchone was used) into the reactor. The fuel is pushed towards the reaction sphere with an auxiliary N_2 flow and meets the O_2/N_2 primary flows just before the JSR injectors to avoid premature fuel oxidation. The gas flow rates were controlled by mass flow controllers (Brooks). The whole assembly is maintained at a temperature higher than the boiling point of the fuel (467 K) to facilitate the fuel evaporation. A probe coupled with a thermocouple (0.1 mm Pt-Pt/Rh-10%), inserted into a thin-walled fused silica tube to avoid any catalytic reactions on the metallic wires, allows the sampling at each desired temperature. To ensure the homogeneity of the mixture, the probe can be moved along the vertical axis of the reactor and the temperature gradient was measured to be less than 2 K cm^{-1}.

At each selected temperature point, the reaction mixture was sampled using a low-pressure fused silica sonic probe. The samples were sent to the analysers through a heated Teflon line maintained at 160°C. These samples are analysed using a Thermo Nexus 670 spectrometer (10 m path length, resolution 0.5 cm^{-1}, 200 mbar in the cell). The gas samples can also be stored at low-pressure in Pyrex bulbs for off-line gas chromatography analysis. Two types of detector were used. A TCD detector coupled to a CP-Carboplot-P7 capillary column allows the quantification of O_2. A FID detector using a CP-Al_2O_3-KCl column in a Shimadzu GC-MS 2010 Plus and a CP-SIL 5CB coupled to DB1 column was used to measure hydrocarbons and oxygenated compounds. Both chromatographs are coupled with a mass spectrometer operating with electron impact ionization (70 eV) for product identification. The different acronyms are listed in Table 2.

Table 2: List of acronyms.

FID	Flame Ionization Detector
GC-MS	Gas Chromatography- Mass Spectrometry

TCD	Thermal conductivity detector
FTIR	Fourier-Transform Infrared Spectrometry
HPLC	High-Pressure Liquid Chromatography
CP-SIL	ChromPack-DimethylpolySiloxane Column
CP-Al_2O_3-KCl	ChromPack Aluminium Oxide Column deactivated by Potassium Chloride
CP-Carboplot-P7	ChromPack Carbon-Based Porous Layer Open Tubular Column

The species quantified in this study are final products and stables intermediates such as H_2, CH_4, C_2H_4, C_2H_6, C_3H_6, allene, propyne, isoprene, methyl cyclopentadienes, benzene, or toluene were measured by gas chromatography. Few other oxygenated species were also quantified including fenchone, acetone, acetaldehyde, acrolein, methacrolein, and methyl vinyl ketone. H_2O, CO, CO_2, CH_2O were measured by online FTIR. The carbon balance was checked for each sample and found to be within ±15%. The uncertainty on reactants and N_2 flow rates was <5%, which has an impact on the residence time and the measured mole fractions [21, 22]. Several heavier hydrocarbons, with one or more double bonds, were separated by GC but their identification was not possible. According to their global formulae, using the equivalent carbon method, their mole fractions were typically < 10 ppm.

3. Kinetic mechanism

The kinetic sub-mechanism of fenchone, a summary of the most important reactions of which is presented in SM1, was developed and integrated into our C_5 mechanism [23]. We have considered the formation of all six possible radicals even though F1 and F2 are very unlikely to be formed under our operating conditions due to higher BDEs [18]. This sub-mechanism was mostly developed following the commonly accepted reaction classes, and the RMG website [24] was used in order to evaluate some rate constants and thermochemistry. As a first and simplified approach, F3 and F4 were considered as equivalent, contrary to F1, and are thus

supposed to be formed at the same rate. Similarly, F5 and F6 were also both considered as equivalent, F6 being formed twice as much as F5 because of the number of available H atoms.

Unimolecular initiation reactions by C–H bond breaking were taken from RMG website considering a pressure dependency (rates at 10 atm were considered in this work). Bimolecular initiation steps were also considered and taken from RMG. The formation of biradicals was found to be negligible under our conditions and thus not included.

For hydrogen abstraction reactions by H atoms, presented in Figure 2 (left), and CH_3 radicals, the rate constants calculated by Sirjean et al. (for norbornane) [19] were used as best analogy for the formation of radicals F3 and F4. For radicals F5 and F6, analogies with respect to similar sites in alkanes were considered. For F1 and F2, rate constants proposed on the RMG website were kept.

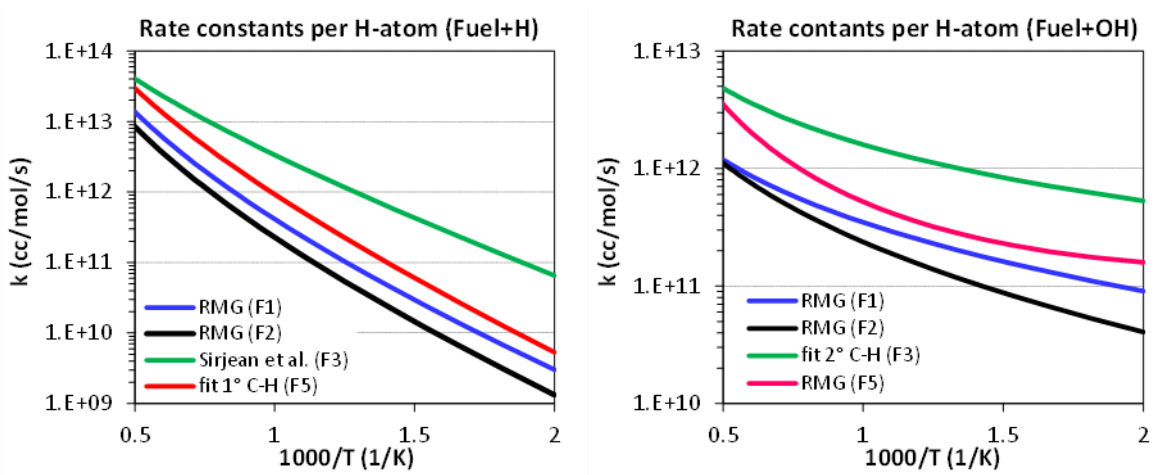

Figure 2. Rate constants for H-abstraction reactions by H (left) and OH (right). F3 and F4 are supposed to have the same rate constants while F6 has twice that of F5.

For H-abstraction reactions by OH radicals, also shown on Figure 2 (right), rate constants suggested by RMG were chosen except for the F3 and F4 radicals (with bond energies similar

as a secondary C–H site in an alkane) where RMG generated rate constants were the same as that for F1 radical. For these secondary C–H sites, rate constants used for alkanes were preferred. These rate constants referred to as 'fit' in the legend of Figure 2 are typical rate constants that can be used for alkanes for H-abstraction reactions. These are obtained by considering several rate constants from the literature (references to these rate constants and the fits for each C–H site can be found in the supplementary material) and fitting them over a wide temperature range.

Rate constants of the beta-scission and internal H-transfer reactions of the fuel radicals, were evaluated through RMG website [24]. Once the 6 primary radicals (F1 to F6) are decomposed, the rate constants of the reactions involved in the consumption/formation of the subsequent species were also taken from RMG website with no modifications. The reaction of resonantly stabilized radicals with HO_2, yielding an aldehyde (or a ketone) and a smaller radical, was considered with a rate constant of 4.50×10^{12} mol cm^{-3} s^{-1}.

Thermochemical properties of all species included into our mechanism were evaluated through group additivity method implemented in RMG [22] as well. However, it was necessary to revise the estimated thermochemistry for radicals F1, F2, and F3 considering the differences observed on bond dissociation energies with what was expected (see Introduction). Ab initio electronic structure calculations at the CBS-QB3 level of theory implemented in Gaussian 16 [25] and isodesmic reactions were used to get more accurate results in terms of BDEs. The mechanism file, thermochemistry file, nomenclature and SMILES notations of these species are provided as supplementary material.

4. Results and discussion

The present section presents a wide range of experimental conditions performed at a constant mean residence time of 0.7s and a constant pressure of 10 atm. Three different equivalence ratios were investigated from fuel-lean to fuel-rich (φ = 0.5, 1, 2). The initial mole fraction of fenchone was set to 1000 ppm for the whole experiment, and the temperature ranged from 700 to 1180 K.

More than 30 species were detected including alkanes (C_1-C_3), alkenes (C_2-C_5), dienes (C_4-C_6), cyclic olefins, aromatics, and oxygenated compounds. Figure 3 illustrates the evolution of the reactants as a function of the temperature where it can be observed that the reactivity starts just below 800 K independently of the equivalence ratio. Moreover, the fuel conversion for the fuel-lean mixture appears to be substantially higher than that of the fuel-rich mixture. The developed kinetic mechanism captures well the onset of the reactivity as well as the fuel consumption for the fuel-lean and the stoichiometric mixtures, but predicts a slightly excessive reactivity between 900-1050 K for the fuel-rich mixture.

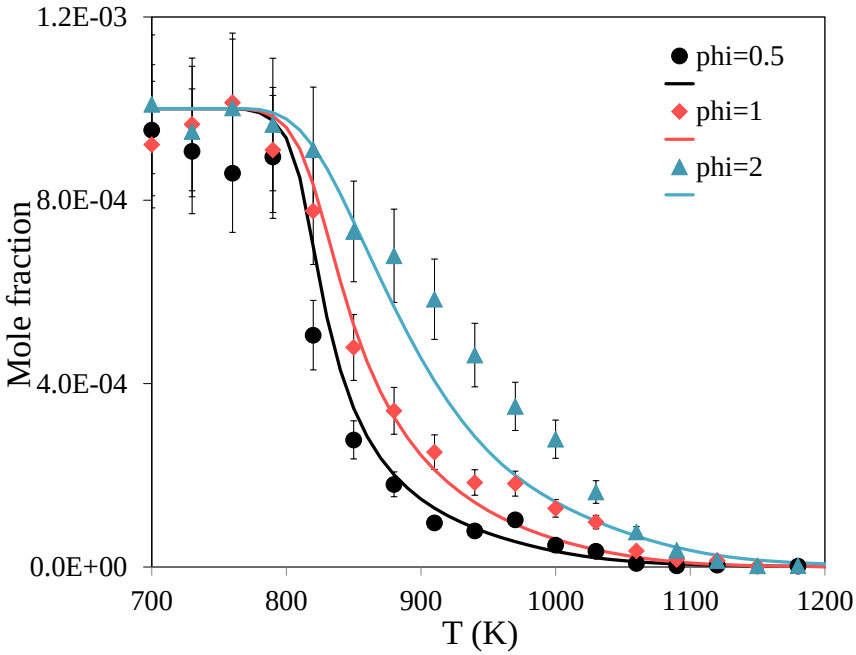

Figure 3. Evolution of the mole fractions of fenchone as a function of temperature for three different equivalence ratios at p = 10 atm, τ = 0.7 s.

The evolution of the mole fractions of the reactants (Fenchone and O_2), and major species are presented in Figure 4. The major intermediate species are CH_4, C_2H_4, and CH_2O whose maximum mole fractions are 2000 ppm and 1750 ppm for CH_4 and C_2H_4 respectively for the rich mixture, whereas formaldehyde is in the order of 180 ppm for all mixtures. As expected, the concentrations of aromatic species increase with the equivalence ratio, the most abundant one being benzene. At φ = 2, its mole fraction reaches almost 200 ppm, while it is only 20 ppm at φ = 0,5. Toluene and xylene were also identified in comparable proportions, their mole fractions being the highest for the fuel-rich mixture. Less than 10 ppm of styrene were also detected at φ = 2 and trace amounts in the other conditions. Low quantities of several cyclic species were also observed, such as cyclopentadiene and two different methyl-cyclopentadiene which are formed with similar mole fractions. Finally, among the oxygenated intermediates, acetone, acrolein, methyl vinyl ketone, and methacrolein were also quantified, their mole fractions being higher under fuel-lean conditions.

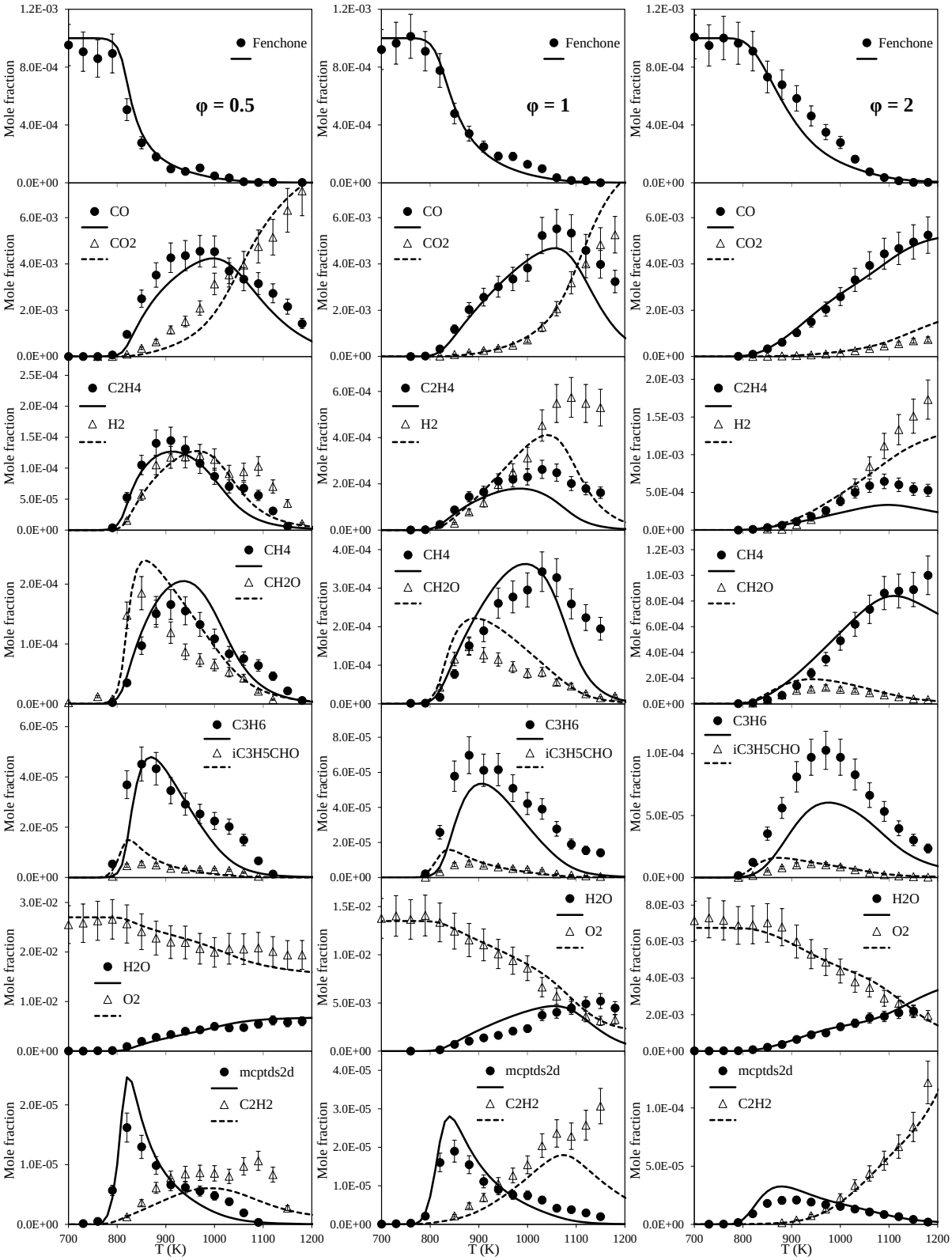

Figure 4. Evolution of the mole fractions of fenchone, O_2, and several stable products as a function of temperature for three different equivalence ratios at p = 10 atm, τ = 0.7 s.

As can be seen from Figure 4, the developed kinetic mechanism captures well the general trend of the fuel consumption as well as the formation and consumption of the different intermediates. Experimentally, it can also be observed that the reactivity slightly decreases (or, at least, does not keep increasing with the temperature) over the temperature range 900-1050 K. This decrease is more and more pronounced when the equivalence ratio increases. It can possibly be attributed to the accumulation of heavy stable intermediates which were not experimentally detected. This decrease in reactivity is not really captured by the model and a more accurate prediction of this phenomenon would constitute a significant improvement of the understanding of the oxidation of fenchone at high temperature. Nevertheless, considering the good agreement observed between calculations and experiments at lower temperature, a reaction pathway analysis was performed under stoichiometric condition and T = 850 K (temperature at which half of the fenchone is consumed) to unravel the major consumption routes of fenchone under these conditions. The result of this reaction pathways analysis is presented in Figure 5.

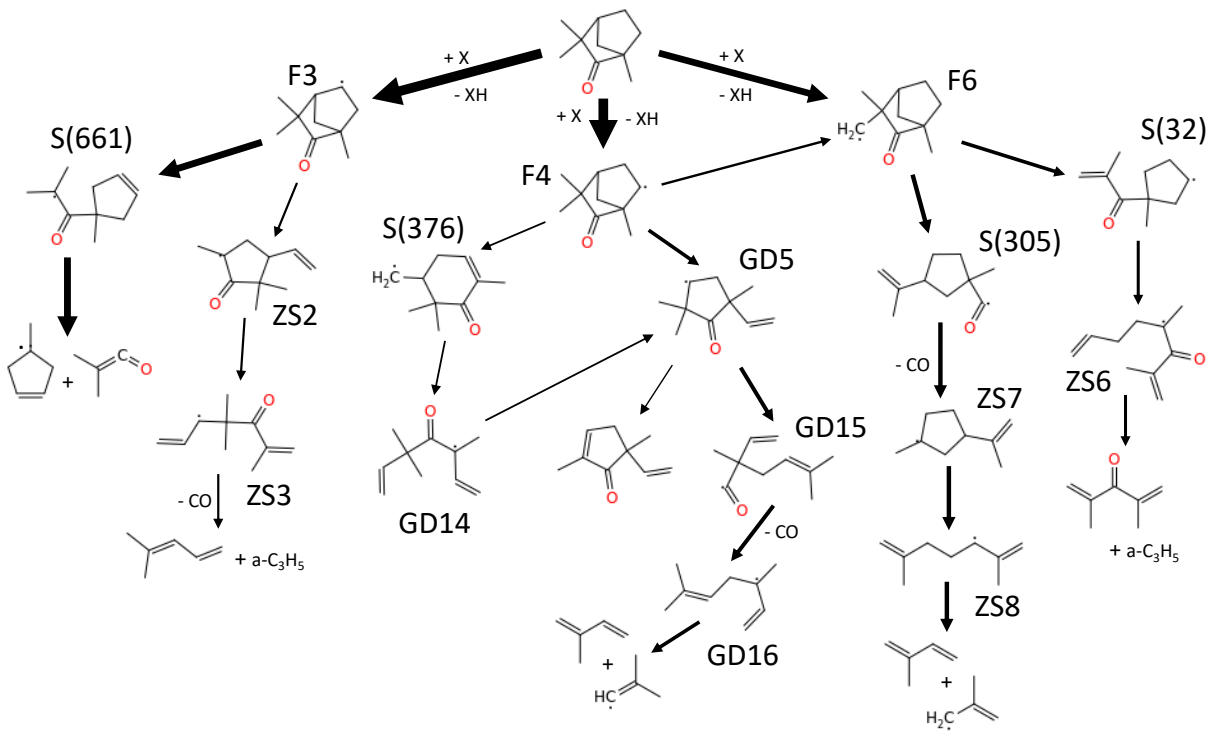

Figure 5. Reaction pathways analysis for the oxidation of fenchone at $\varphi = 1$, $p = 10$ atm, $\tau = 0.7$ s, and $T = 850$ K. Arrow thickness denotes the intensity of respective carbon flux.

As illustrated by Figure 5, fenchone is mainly consumed by H-abstraction reactions by OH yielding F3 and F4 at the same rate. Though being less formed than the two previous, F6 is the third most important primary radical in this analysis, F5, F1, and F2 being almost negligible (9%, 5%, and 4% respectively). The fate of F3, F4, and F6 is discussed in the following:

F3- Almost three quarters of F3 decompose into 4-isobutenoxy-4-methyl-1-cyclopentene, S(661), which reacts completely to yield a methyl cyclopentenyl radical and opens the route to benzene, which will be elaborated in the next paragraph. The remaining quarter leads to allyl radical and methyl pentadiene which was not observed experimentally. The third possible C-C β-scission, opening the bridge over the six-membered ring and yielding a radical of a ramified cyclohexanone, appears to be negligible under these conditions.

F4- A quarter of F4 isomerizes into F6, while more than a third produces GD5 (C=CC1(C)C[CH]C(C)(C)C(=O)1). The latter is also formed by cyclization of a radical obtained from the 6-membered ring opening. A quarter of GD5 yields a ramified cyclopentenone, the rest producing isoprene and the vinylic isobutenyl radical after ring opening and decarbonylation. This isobutenyl radical is mostly responsible for the formation of acetone. Two other C-C β-scission reactions were considered to consume F4, but it turns out that they are both negligible under these conditions.

F6- The two pathways consuming F6 are similar in terms of flow rate. One yields isoprene after decarbonylation and ring opening, whereas the other one produces diisopropenyl ketone, which was not observed experimentally. A third C-C β-scission was also considered for F6 producing CH_3 radicals, but turns out to be negligible because of its high activation energy resulting from RMG rate rules.

In order to complete the picture we have of the reactivity of fenchone, a sensitivity analysis on the fuel was carried out at 770 K for the stoichiometric mixture. As can be seen from Figure 6, under these conditions, fenchone consumption is mostly sensitive to H-abstraction reactions by HO_2, and CH_3O_2 to a lesser extent, yielding radicals F3 and F4, i.e. the secondary radicals. Therefore, fenchone is also sensitive to reactions producing or consuming HO_2 and H_2O_2. More interestingly, fenchone oxidation is also sensitive to ring opening reactions such as F3 into ZS2 or C9H15(38) = C9H15(392) (see Fig. 5 and supplementary material for structures).

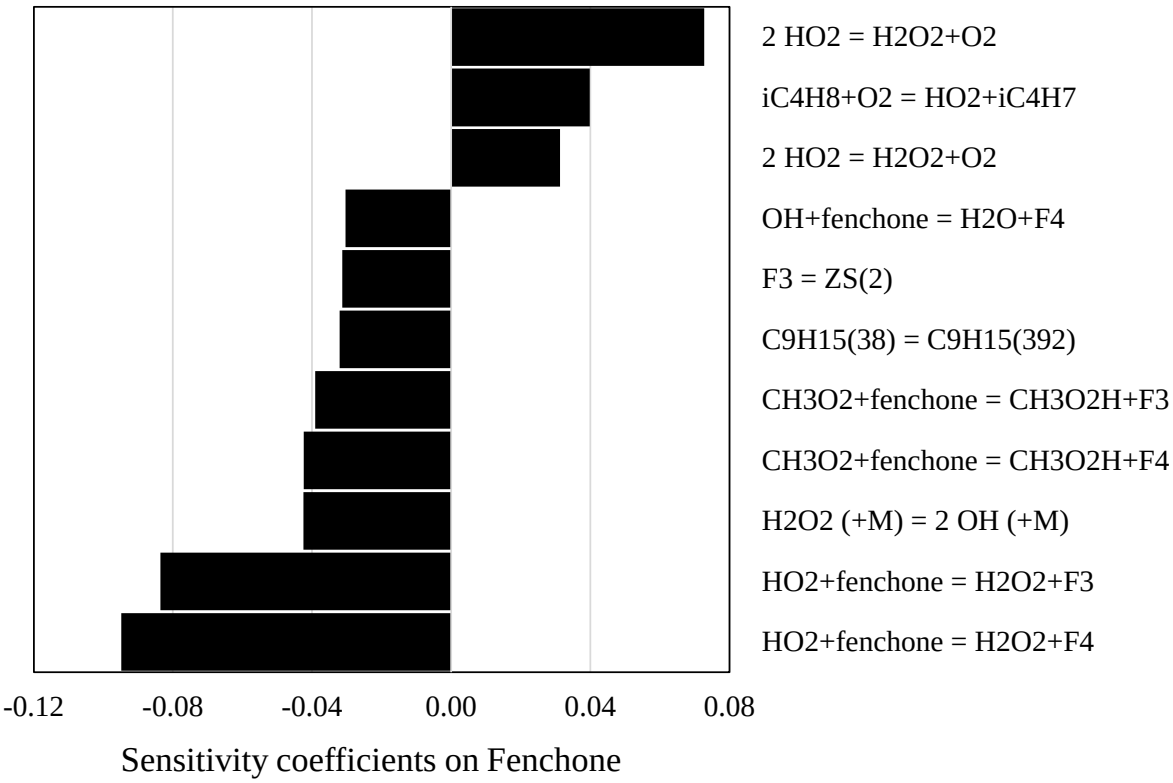

Figure 6. Sensitivity analysis on fenchone at $\varphi = 1$, p = 10 atm, $\tau = 0.7$ s, and T = 770 K.

Benzene was produced in significant amounts during the oxidation of fenchone. Other aromatic compounds such as toluene, styrene, xylenes, trimethyl benzenes or methyl styrene were also observed especially under fuel-rich conditions. Unfortunately, our kinetic mechanism is not developed to model the formation and consumption of aromatic species, and improvements on the basis of the present results would be too limited. However, the particular

case of benzene represents a way of possible improvements to better understand the different steps occurring during this process. Figure 7 illustrates how benzene is overestimated by the model under fuel-lean conditions but under estimated at high temperature under fuel-rich conditions. A reaction pathway analysis was performed at φ = 1 and T = 950 K, revealing that benzene is mostly produced by the reactions of methyl cyclopentenyl radicals, methyl cyclopentadienes, methyl cyclopentadienyl radicals, and fulvene. This rate of production analysis is presented in Figure 8 where it can be seen that benzene mostly comes from radical F3 through the formation of methyl cyclopentenyl radicals. Our kinetic mechanism has been significantly modified, in order to account for recent CH_3+C_5H_5 rate constant calculations by Krashnoukov et al. [26], but efforts are still required to better represent benzene accumulation under these conditions, given the diversity of C_6 intermediates and the corresponding benzene formation and consumption pathways [27].

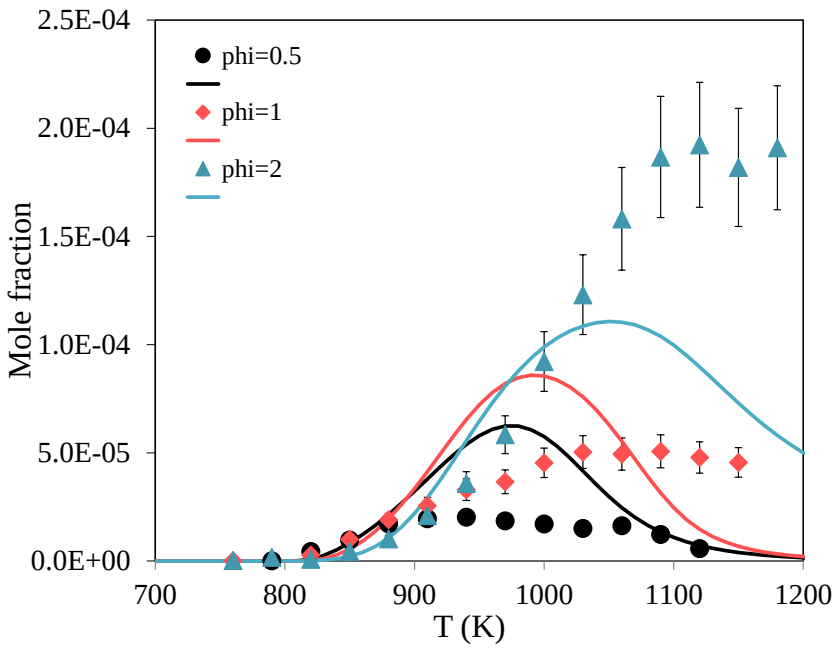

Figure 7. Evolution of the mole fractions of benzene as a function of temperature for three different equivalence ratios at p = 10 atm, τ = 0.7 s.

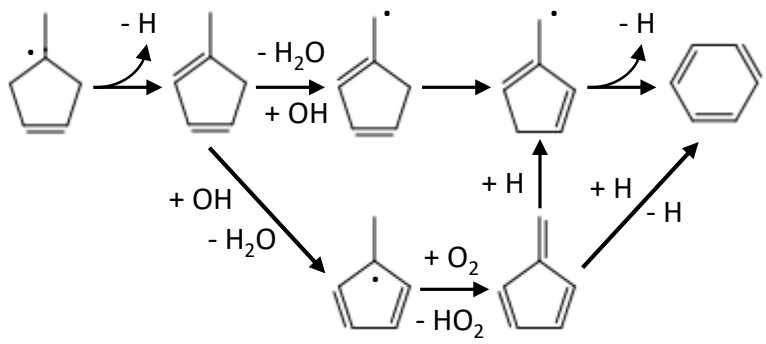

Figure 8. Routes of formation of benzene at p = 10 atm, τ = 0.7 s, and φ = 1.

Conclusions

In the present study, we have investigated the oxidation chemistry of fenchone via detailed speciation experiments in a jet-stirred reactor. Fenchone is a strained-ring hydrocarbon with potentially interesting characteristics (e.g. high energy density) and as a high-octane component however its oxidation chemistry has not been dissected before. A detailed kinetic sub-mechanism of fenchone is also developed mostly using the RMG website and complementary structure/reactivity relations with similar hydrocarbons when available. Three equivalence ratios were chosen for the experiments in order to assess the differences in reactivity. In terms of fuel conversion, the fuel-rich mixture was found to be the least reactive one, and is also the one that produced more benzene. Reaction pathway analyses showed that benzene formation is closely linked to the chemistry of methyl cyclopentenyl radicals, methyl cyclopentadiene isomers, methyl cyclopentadienyl radicals, and fulvene. These could constitute future targets for model improvement. Apart from benzene, toluene as well as traces of styrene were identified as aromatic species. Among potential oxygenated pollutants, formation of acrolein and methacrolein is observed. Overall, the kinetic mechanism showed good agreement with the present experimental data and helped us identify the underlying reaction pathways. Further

perspectives could be the investigation of global combustion properties of fenchone in environments close to engine operation such as ignition delay times.

Acknowledgement

Support from the CAPRYSSES project (ANR-11-LABX-006-01) funded by the PIA (Programme d'Investissement d'Avenir) is gratefully acknowledged. The authors thank Aramco Overseas Company for supporting this research.

References

[1] Ausfelder F, Wagemann K. Power-to-Fuels: E-Fuels as an Important Option for a Climate-Friendly Mobility of the Future. Chem Ing Tech 2020;92(1-2):21-30.

[2] Meylemans HA, Quintana RL, Harvey BG. Efficient conversion of pure and mixed terpene feedstocks to high density fuels. Fuel 2012;97(Supplement C):560-568.

[3] Zaabi AA, Raj A, Elkadi M, Anjum D, Li L, George A, Shebli MNA. Effects of the addition of a high energy density fuel, adamantane to diesel on its cetane number, sooting propensity, and soot nanostructural properties. Cleaner Chemical Engineering 2022;2:100008.

[4] Vandewiele NM, Magoon GR, Van Geem KM, Reyniers M-F, Green WH, Marin GB. Kinetic Modeling of Jet Propellant-10 Pyrolysis. Energy & Fuels 2015;29(1):413-427.

[5] Abdrabou MK, Morajkar PP, Guerrero Peña GDJ, Raj A, Elkadi M, Salkar AV. Effect of 5-membered bicyclic hydrocarbon additives on nanostructural disorder and oxidative reactivity of diffusion flame-generated diesel soot. Fuel 2020;275:117918.

[6] Salamanca M, Botero ML, Martin JW, Dreyer JAH, Akroyd J, Kraft M. The impact of cyclic fuels on the formation and structure of soot. Combust Flame 2020;219:1-12.

[7] Andrews RJ, Smith CF, Alexander AJ. Mechanism of carbon nanotube growth from camphor and camphor analogs by chemical vapor deposition. Carbon 2006;44(2):341-347.

[8] Barrientos EJ, Lapuerta M, Boehman AL. Group additivity in soot formation for the example of C-5 oxygenated hydrocarbon fuels. Combust Flame 2013;160(8):1484-1498.

[9] Morajkar PP, Guerrero Peña GDJ, Raj A, Elkadi M, Rahman RK, Salkar AV, Pillay A, Anjana T, Cha MS. Effects of Camphor Oil Addition to Diesel on the Nanostructures and Oxidative Reactivity of Combustion-Generated Soot. Energy & Fuels 2019;33(12): 12852-12864.

[10] Gao CW, Vandeputte AG, Yee NW, Green WH, Bonomi RE, Magoon GR, Wong H-W, Oluwole OO, Lewis DK, Vandewiele NM, Van Geem KM. JP-10 combustion studied with shock tube experiments and modeled with automatic reaction mechanism generation. Combust Flame 2015;162(8):3115-3129.

[11] Zhong B-J., Zeng Z-M., Zhang H-Z. An experimental and kinetic modeling study of JP-10 combustion. Fuel 2022;312:122900.

[12] Parsinejad F, Arcari C, Metghalchi H. Flame Structure and Burning Speed of JP-10 Air Mixtures. Combust Sci Technol 2006;178(5):975-1000.

[13] Coudour B, Chetehouna K, Courty L, Garo JP, Lemée L, Mounaïm-Rousselle C, Halter F. Combustion Characteristics of Two Biogenic Volatile Organic Compounds: L-Fenchone and 3-Hexen-1-ol. Combust Sci Technol 2014;186(10-11):1284-1294.

[14] Courty L, Chetehouna K, Halter F, Foucher F, Garo JP, Mounaïm-Rousselle C. Experimental determination of emission and laminar burning speeds of α-pinene. Combust Flame 2012;159(4):1385-1392.

[15] Sato T, Murata K, Nishimura A, Tsuchiya T, Wasada N. Pyrolysis of organic compounds-II: The flash pyrolysis of camphor and its related compounds. Tetrahedron 1967;23(4):1791-1798.

[16] GNN, https://gnn.avt.rwth-aachen.de [accessed May 2023].

[17] Li R, Herreros JM, Tsolakis A, Yang W. Machine learning-quantitative structure property relationship (ML-QSPR) method for fuel physicochemical properties prediction of multiple fuel types. Fuel 2021;304:121437.

[18] Wang H, Zhang B, Gong S, Wang L, Zhang X, Liu G. Experimental and modeling studies of quadricyclane and 2-ethylnorbornane pyrolysis from atmospheric to high pressure. Combust Flame 2021;226:163-181.

[19] Sirjean B, Herbinet O, Glaude PA, Ruiz-Lopez M, Fournet R. Theoretical Study of the Thermal Decomposition of a Jet Fuel Surrogate. Proc. WSS/CI Spring 2008 Meeting Paper #08-S11.

[20] Dagaut P, Cathonnet M, Rouan JP, Foulatier R, Quilgars A, Boettner JC, Gaillard F, James H. A jet-stirred reactor for kinetic studies of homogeneous gas-phase reactions at pressures up to ten atmospheres (≈1 MPa). J Phys E: Scientific Instruments 1986;19(3):207.

[21] Thion S, Togbé C, Serinyel Z, Dayma G, Dagaut P. A chemical kinetic study of the oxidation of dibutyl-ether in a jet-stirred reactor. Combust Flame 2017;185: 4-15.

[22] Thion S, Serinyel Z, Dayma G, Dagaut P. More insight into cyclohexanone oxidation: Jet-stirred reactor experiments and kinetic modeling. Fuel 2018;220: 908-915.

[23] Dayma G, Thion S, Serinyel Z, Dagaut P. Experimental and kinetic modeling study of the oxidation of cyclopentane and methylcyclopentane at atmospheric pressure. Int J Chem Kinet 2020;52(12): 943-956.

[24] RMG, https://rmg.mit.edu/; 2022 [accessed September 2022].

[25] M. J. Frisch, G. W. Trucks, H. B. Schlegel, et al., Gaussian, Inc., Wallingford CT, 2016.

[26] Krasnoukhov VS, Porfiriev DP, Zavershinskiy IP, Azyazov VN, Mebel AM. Kinetics of the CH3 + C5H5 Reaction: A Theoretical Study. The Journal of Physical Chemistry A 2017;121(48):9191-9200.

[27] Hansen N, Kasper T, Yang B, Cool TA, Li W, Westmoreland PR, Oßwald P, Kohse-Höinghaus K. Fuel-structure dependence of benzene formation processes in premixed flames fueled by C6H12 isomers. Proc. Combust. Inst. 2011;33(1):585-592.